Characterization of a Major Fraction of Disordered All-Trans Chains in Cold-Drawn High-Density Polyethylene by Solid-State NMR

D. M. Mowery,[†,‡] D. J. Harris,[†,§] and K. Schmidt-Rohr*

Department of Polymer Science and Engineering and Materials Research Science and Engineering Center, University of Massachusetts, Amherst, Massachusetts 01003, and Department of Chemistry and Ames Laboratory, Iowa State University, Ames, Iowa 50011

Received June 24, 2005; Revised Manuscript Received February 11, 2006

ABSTRACT: In cold-drawn, necked high-density polyethylene, solid-state nuclear magnetic resonance (NMR) has identified a major fraction of chain segments intermediate to the ordered crystalline and the almost isotropic amorphous phases. This partially mobile and disordered all-trans fraction in the strain-hardened sample contains $38 \pm 6\%$ of all chain segments in the bulk. Thus, it represents the second largest component in the system, ahead of the disordered gauche-containing or amorphous ($17 \pm 4\%$) and the monoclinic crystalline ($4 \pm 2\%$) phases. A series of one- and two-dimensional NMR experiments, several of which make use of an "inverse ^{13}C T_1 relaxation time filter" for selective observation of the intermediate-component signals, show the intermediate component (or components) to consist of all-trans chains with disordered packing. While the crystalline component has a standard deviation of the chain axis from the draw direction of 1°, the intermediate components exhibit an ~8° spread of chain-axis orientations from the draw axis. The chains in the intermediate components undergo fast rotational motions around their axes, with motional amplitudes of ca. 20°.

1. Introduction

A sound qualitative and quantitative understanding of the component microstructure in mechanically deformed and oriented semicrystalline polymers is crucial for analyzing and predicting the physical performance of these materials. Such knowledge forms the basis of modeling anisotropic mechanical behavior in terms of distinct components found in the oriented polymer morphology, e.g., crystalline and amorphous.[1−5] The application of component modeling to practical engineering tasks is of great interest in the effective development of enhanced materials and products. For example, the creep of micrometer-sized craze fibrils located at a growing crack tip has been recognized as a major mechanism in the mechanical failure of polyethylenes by slow crack growth. This fibril creep has been modeled with the creep performance of macroscopic, cold-drawn polyethylene (PE) samples.[6−9] A more thorough grasp of the component morphology of cold-drawn PE could give a better understanding of the slow crack growth phenomenon. Correlating the size, amount, and arrangement of the morphological components with creep response may be useful in the production of PE resins with superior stress crack resistance.

The morphological structure of drawn semicrystalline polymers is considerably more complex than can be described by a simple two-phase model.[3,10−14] When high-density polyethylene (HDPE) is uniaxially deformed at ambient temperature (i.e., cold drawn) and necked, the original spherulitic arrangement of lamellar crystallites is dramatically transformed into a highly oriented, fibrillar microstructure with molecular chains that are mostly parallel to the draw axis. It is generally agreed that the crystalline lamellae are broken into small "mosaic" blocks during necking. Hence, to account for the mechanical integrity and increased strength along the draw direction, various morphological structures such as tie molecules[3,10,12] and intercrystalline bridges[15] have been invoked and incorporated into the classical two-phase model, yielding more intricate representations of the anisotropic morphology of drawn and oriented polyethylenes.

Recent analyses of cold-drawn and necked HDPE samples using Raman scattering[8,16,17] have revealed all-trans fractions exceeding the measured crystallinity significantly. The increased presence of noncrystalline all-trans chains was attributed to morphological disordering during the necking process. However, distinct spectroscopic peaks of the noncrystalline trans component have not been directly observed in cold-drawn HDPE. In addition, its orientation, conformational order, molecular mobility, and chain packing still need to be characterized. Even the crystallinity of cold-drawn polymers is difficult to determine since the orientational order, the nonequilibrium nature of the necked microstructure, and unknown details of the intricate morphology make interpretations of DSC, density, WAXD, SAXS, and Raman scattering measurements difficult.

In this paper, we report the quantitative spectroscopic characterization of the morphological composition of cold-drawn, necked and strain-hardened HDPE using various solid-state nuclear magnetic resonance (NMR) techniques. The undrawn, melt-crystallized HDPE "precursor" is used as a reference, to show the effects of cold drawing on the microstructure. Of greatest significance is the detection of a major fraction of disordered all-trans chains in the necked microstructure of cold-drawn HDPE, with properties distinct from those of the crystalline and amorphous phases. At the draw ratio $\lambda > 16$, this "intermediate" (but not necessarily interfacial) material will be shown to represent the second largest fraction in the morphology, ahead of the disordered gauche-containing (i.e., amorphous) and the monoclinic crystalline phases. By a series of NMR experiments, of which several utilize an "inverse ^{13}C T_1 filter" that enables selective observation of the signals of the various components, the characteristic molecular conforma-

* To whom correspondence should be addressed at Iowa State University. Telephone: 515-294-6105. Fax: 515-294-0105. E-mail: srohr@iastate.edu.
[†] University of Massachusetts.
[‡] E-mail: dmmower@sandia.gov.
[§] E-mail: douglas.harris@cytec.com.

10.1021/ma0513517 CCC: $33.50
Published on Web 03/23/2006

tion, mobility, and orientation distribution of the intermediate component(s) will be examined.

2. Experimental Section

2.1. Material Characteristics and Sample Preparation. A commercial copolymer of ethylene and 1-octene (Dow HD-12450N) was used in our study, but the comonomer concentration and small-chain branching content are very minor (<0.5 mol %; no ^{13}C signals of branches were detected in solid-state NMR spectra). This specific material was selected for its overall linear molecular structure (as indicated by its comparatively high ambient density, 0.952 g/cm^3) and relatively low molecular weight ($M_n \sim 3 \times 10^4$). According to Popli and Mandelkern,[18] the draw ratio at break for conventional linear polyethylenes at room temperature increases with decreasing molecular weight. This particular HDPE grade is synthesized with a molecular weight distribution (PDI $\sim$ 2.5) that is narrower than that of most commercial linear HDPE resins, thereby reducing the potentially undesirable complications of multiple chain lengths in these studies.

Compression-molded test sheets (1.97 $\pm$ 0.04 mm thick) of the HDPE were prepared according to ASTM Standard Practice D 1928-90 Procedure C. A molding pressure of approximately 4.3 MPa was used. A cooling rate of 15 $\pm$ 4 °C/min was maintained. Samples designated as "undrawn" in this paper were extracted directly from the molded sheets. Standard dumbbell-shaped test specimens were punched from the molded sheets. The specimen shape and dimensions conformed to the Type V design outlined in ASTM Standard Test Method D 638. Using an Instron model 1123 screw-driven tensile tester, specimens were drawn at 2 mm/min (0.0013 s^{-1}) to an extensional change of 240 mm (or nominal drawing strain of 945%), which is just before the fracture of the material at 264.8 $\pm$ 9.7 mm (1040 $\pm$ 40% drawing strain). At this extension, a test specimen was completely necked along its tensile length of narrow cross-sectional area and subsequently strain hardened, achieving significant molecular orientation along the tensile draw direction. Samples with a draw ratio $\lambda > 16$ were obtained. Samples designated as "drawn" in this paper were cut from these necked specimens. All drawing was done at room temperature (21 $\pm$ 1 °C). Before any further testing, drawn samples were allowed to freely and sufficiently relax and recover at room temperature for at least a week after unloading from the drawing tension.

2.2. Non-NMR Determination of Component Composition. Differential scanning calorimetry (DSC) measurements were performed to quantify crystallinity in undrawn samples of the HDPE. A TA Instruments model 2910 DSC was employed. First heats were analyzed at 10 °C/min using a sample mass of 5−10 mg. A heat of fusion for the perfect PE crystal of 293 J/g was used in calculating mass-percent crystallinity values from the measured sample heats of fusion.[19]

FT-Raman scattering measurements were made to determine mass percentages of the crystalline, amorphous, and intermediate components in undrawn HDPE samples following the method of Strobl and Hagedorn.[20] Crystallinity was computed using the band at 1416 cm^{-1} and the amorphous content from the 1303 cm^{-1} band. A Bruker FRA 106 instrument equipped with a Nd:YAG (1.064 μm) laser at 250 mW was used in this work; spectral resolution was 4 cm^{-1}. Spectral curve fitting and calculations were done with PE-GRAMS/2000 software. On the basis of the recommendations of Rull et al.,[21] all bands were freely fit by the software with mixtures of Gaussian and Lorentzian functions. Only the position of the low, broad band at 1270 cm^{-1} was fixed. The method of Strobl and Hagedorn[20] cannot be applied to the cold-drawn, oriented PE sample due to molecular orientation effects, as demonstrated in the work of Lagaron et al.[8]

2.3. NMR Parameters. Solid-state NMR experiments were conducted using a Bruker DSX 300 spectrometer (B_o = 7 T) at a ^{13}C resonance frequency of 75.48 MHz. Measurements were made under both static and magic-angle spinning (MAS) conditions at ambient temperature. For all MAS experiments, 4 mm diameter zirconia rotors with Kel-F caps were used to hold the samples; a 5-kHz spinning speed and decoupling with two-pulse phase modulation (TPPM)[22] at $\gamma B_1/2\pi$ = 62.5 kHz were utilized. A ^{13}C 90° pulse length of 4−5.5 μs was employed in ^{13}C direct-polarization (DP) experiments. For standard cross-polarization (CP) measurements, both static and under MAS, a ^1H 90° pulse length of 4 μs, and a contact time of 0.5 ms were applied. A 90° pulse length of 3.85 μs was used with ^1H wide-line measurements.

Two-dimensional (2D) wide-line separation (WISE) NMR experiments[23] conducted in this study utilized a magic-angle spin lock (MASL) on ^1H during CP following the method of Lee and Goldburg.[24] A recent paper[25] has presented the theoretical background of this method. The small crystallite sizes in the drawn HDPE necessitated the suppression of ^1H spin diffusion during the CP contact pulse, which MASL accomplishes via attenuation of the $^1H-^1H$ dipolar interaction. A ^1H 35° pulse after the t_1 delay in the WISE pulse sequence brings the ^1H magnetization to the magic angle with respect to the B_o field. ^1H were pulsed off resonance during CP so that the effective field B_{eff} would be at the magic angle with the B_0 field, and $\gamma B_{eff}/2\pi$ = 63 kHz. A shorter CP contact time (0.2 ms) was also used.

Samples of the HDPE were wrapped in Teflon tape for better packing and alignment during ^{13}C NMR measurements. However, for experiments with ^1H detection, no Teflon tape was used, as additives in some Teflon tapes were found to produce undesirable ^1H signals. In most measurements under MAS, the draw directions of pieces from the necked samples were aligned parallel to the long axis of the sample rotor and, hence, the sample coil.

Static measurements of the oriented sample were performed in the static NMR probe for the 0 and 90° orientations. Pieces of the necked material were bundled with Teflon tape so that their draw directions were parallel with each other and snuggly fit into the sample coil, whose long axis is perpendicular to the B_o field, with draw directions either parallel (90° orientation) or perpendicular (0° orientation) to the coil axis. For the 55° orientation, the MAS probe was utilized without sample spinning. Pieces of the necked material were packed into a 4 mm MAS rotor with the draw directions parallel to rotor axis and, hence, at the magic angle (55°) to the B_o field.

To eliminate effects of sample orientation in some experiments, macroscopically isotropic samples were prepared from the drawn material by carefully cutting it into small flakes. For static experiments, these flakes were loosely packed into a 4 mm glass tube that was snugly fit into the sample coil of the static NMR probe employed.

2.4. Inverse ^{13}C T_1 Filtering. To characterize intermediate components in the morphology of HDPE, NMR experiments are required that allow its selective observation based not only on its all-trans chemical shift of >32.8 ppm, but also in terms of its distinctive intermediate ^{13}C longitudinal (T_1) relaxation time. In earlier studies of various forms of polyethylene,[26−33] the intermediate $T_{1,C}$ has generally been estimated to differ from the ^{13}C T_1 relaxation times of both the amorphous and crystalline components by at least an order of magnitude. Selective relaxation experiments require suppression of both the crystalline and the amorphous signals, based on these differences in T_1 values. Most traditional experiments do not separate resonances of the crystalline and intermediate components, or of the intermediate and amorphous components. For instance, cross-polarization suppresses the signals of the highly mobile amorphous components, since they have reduced dipolar couplings and CP efficiencies, but retains both crystalline and intermediate resonances.

Single-pulse excitation of ^{13}C can select the mobile components and could be combined with a ^{13}C T_1 filter to retain only the intermediate component(s). However, this procedure reduces the sensitivity greatly, due to the loss of CP enhancement and the necessity of long recycle delays (>5 s) to ensure sufficient relaxation of the magnetization within the intermediate component-(s). In addition, information is not provided with regard to the useful spectral and relaxation properties of ^1H as measured in such

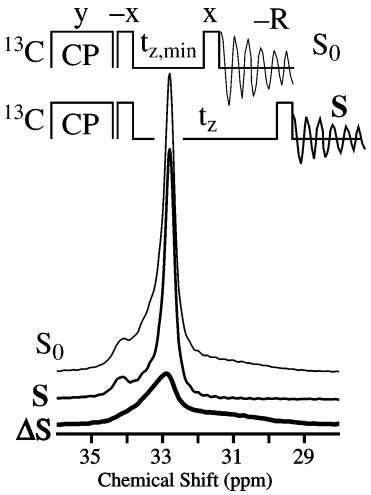

Figure 1. Demonstration of the "inverse $T_{1,C}$ filter" experiment. Utilizing the $T_{1,C}$ filter pulse sequence of Torchia,[34] with variable $T_{1,C}$ filter delay time t_z, an X-second inverse $T_{1,C}$ filtered spectrum ($\Delta\mathbf{S}$) is obtained as the unscaled difference between an *X*-s $T_{1,C}$ filtered spectrum (**S**, where $t_z = X$ s) and a reference spectrum ($\mathbf{S_o}$, where $t_{z,min} = 1$ ms) acquired with the same number of scans. Spectra shown are of the cold-drawn HDPE sample, for $t_z = 10$ s.

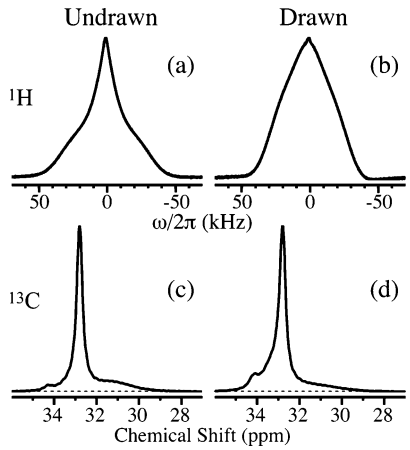

Figure 2. Comparison of standard solid-state NMR spectra of the undrawn and drawn samples (left and right columns, respectively): (a, b) ^{1}H wide-line spectra (without sample rotation); (c, d) ^{13}C CP/MAS spectra.

experiments as WISE and ^{13}C-detected $T_{1\rho,H}$ experiments that rely on ^{1}H−^{13}C correlation through cross-polarization.

Therefore, an "inverse $T_{1,C}$ filter" is introduced here. Utilizing this method, it is now possible to selectively observe the signals of short ^{13}C T_1 magnetization with good CP efficiency. The ^{1}H T_2 and $T_1\rho$ relaxation behavior of the inverse $T_{1,C}$ filtered signals can be easily measured by applying the suitable pulses to ^{1}H before CP. The basic pulse sequence for the inverse $T_{1,C}$ filter is the same as for a traditional ^{13}C T_1 filter[34] (Figure 1). An X-second inverse $T_{1,C}$ filtered spectrum is obtained as the (unscaled) difference between an X-second $T_{1,C}$ filtered spectrum and a reference spectrum obtained with the same pulse program and a very short (1 ms) relaxation delay.

Quantitatively, the spectral intensity after a $T_{1,C}$ filter of duration t_z can be written as the sum of the cross-polarization signals $S_{n,CP}(\omega)$ of the different components, each weighted by $\exp(-t_z/T_{1,n})$, where $T_{1,n}$ is the ^{13}C longitudinal relaxation time of the *n*th component. The difference signal (ΔS in Figure 1) is then

$$S_{\text{invfil}}(\omega,t_z) = \sum_n e^{-0/T_{1,n}} S_{n,CP}(\omega) - \sum_n e^{-t_z/T_{1,n}} S_{n,CP}(\omega)$$
$$= \sum_n (1 - e^{-t_z/T_{1,n}})\, S_{n,CP}(\omega) \quad (1)$$

If the relaxation time of component n_0 is long, $T_{1,n0} \gg t_z$, the signal of that component is canceled, while the signals of other components with short relaxation times are retained. The inverse $T_{1,C}$ filtered spectrum is like a one-pulse spectrum with a recycle delay of duration t_z, where the signal of each specific chemical group is multiplied with its CP efficiency.

In an extension of this concept, differences between spectra for two intermediate times t_{za} and t_{zb} can be taken. This will eliminate the signals of components with short $T_1 \ll t_{za} < t_{zb}$ as well as long $T_1 \gg t_{zb} > t_{za}$, which enables selection and isolation of the signals of components with intermediate $T_{1,C}$ relaxation times. A similar method was employed by Kaji et al.[27] in the acquisition of simple 1D ^{13}C CP/MAS spectra to probe the morphology of UHMW−PE fibers, but it was not systematically combined with other experiments, such as WISE or static line shape measurements, which provide more detailed characterization of intermediate components.

In contrast to many other difference spectra that have been shown in the literature with the aim of isolating the signal of a specific component, no scaling factors are needed to obtain the inverse $T_{1,C}$ filtered spectra. The filter can also be readily incorporated into WISE, ^{1}H spin diffusion, or ^{13}C-detected $T_{1\rho,H}$ experiments, as demonstrated below.

3. Results and Discussion

3.1. Standard Solid-State NMR of the Undrawn and Drawn HDPE. Various 1D NMR experiments were conducted on the drawn HDPE sample. The undrawn, melt-pressed precursor was examined as a reference. Standard ^{1}H wide-line and ^{13}C CP/MAS spectra of the undrawn and drawn samples are presented in Figure 2. Clearly, cold drawing leads to structural changes that are reflected in the spectra. For instance, the ^{1}H spectrum of the undrawn sample (Figure 2a) shows a relatively distinct, motion-narrowed peak due to the amorphous material,[35−37] and a much wider "band" that is identified with the crystalline fractions, while the drawn sample (Figure 2b) displays only very limited line-width contrast between crystalline and amorphous components. Although a component of intermediate line width is not clearly discernible in Figure 2a, an intermediate component has been inferred from such data in past studies[36,37] by fitting the ^{1}H wide-line pattern with mathematical functions based on a three-component model. The ^{1}H wide-line spectra do reveal qualitatively that molecular mobility in the noncrystalline domains has decreased upon cold drawing and necking.

In the ^{13}C CP/MAS spectra (Figure 2, parts c and d), additional intensity appears upon deformation downfield (to the left) of the sharp resonance at 32.8 ppm identified with the orthorhombic crystals.[38] These signals are due to all-trans chains, but with different molecular packing than the orthorhombic crystalline lattice.[39] In the spectral region of the gauche-containing amorphous phase, around 28−32 ppm,[38] indications of line-shape changes due to cold drawing are also observed. The overall intensity of the amorphous signals decreases relative to the crystalline peak, and a slight downfield shift is detectable. Nevertheless, a comprehensive and quantitative inspection into the nature of the microstructural changes induced by cold drawing is very difficult from these standard NMR spectra alone.

***T*$_{1,C}$-Filtered ^{13}C Spectra: Rigid Chain Segments.** More detailed and quantitative information about the polymer morphology can be derived from NMR spectra that are discriminating to specific components in the microstructure. Such selectivity can be achieved by utilizing differences in spin relaxation times, which are usually based on differences in the segmental mobility of the various components. In semicrystalline polymers far above the glass transition of the amorphous domains, a particularly

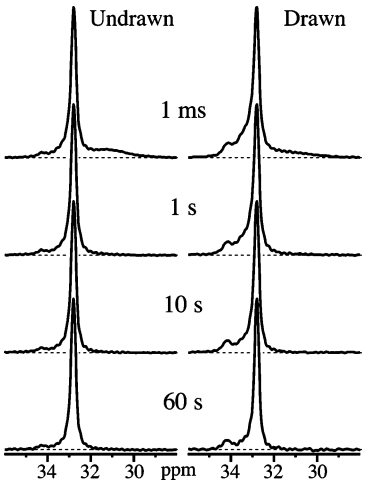

Figure 3. ^{13}C CP/MAS $T_{1,C}$ filtered spectra of the undrawn and drawn samples (left and right columns, respectively) at selected $T_{1,C}$ filter delay times, as indicated. Spectra are scaled so that the intensities of the orthorhombic crystalline peaks (32.8 ppm) are the same.

useful distinction is made according to the ^{13}C longitudinal ($T_{1,C}$) relaxation time. $T_{1,C}$ is shortest for molecular segments moving with rates near the Larmor frequency of ^{13}C, which is 75 MHz in the 7-T B_0 field used in this study. Segments in the amorphous regions have a short $T_{1,C}$, less than one second, due to fast molecular mobility, while the $T_{1,C}$ of the crystallite core exceeds 100 s.[26,40,41] For interfacial regions, intermediate $T_{1,C}$ values are found for a variety of reasons, which prominently include transferred relaxation due to chain diffusion from amorphous to crystalline regions in polyethylene.[42] Note that on the ~10 s scale, magnetization from the amorphous regions does not diffuse far into the crystallites, so the core of the crystallites exhibits no significant short-$T_{1,C}$ signal.

To monitor the ^{13}C T_1 relaxation of the various morphological components, the experiment of Torchia[34] was used. A similar approach has been taken in several studies[26−28,40,43] of crystalline $T_{1,C}$ values in polyethylenes. A series of ^{13}C CP/MAS spectra with varying $T_{1,C}$ filter delay time (t_z in Figure 1) were acquired for the undrawn and drawn samples. The signals of a mobile component will become negligible after a certain relaxation delay.

$T_{1,C}$-filtered spectra of both the undrawn and drawn samples at selected delay times t_z are presented in Figure 3. In both samples, the amorphous magnetization relaxes within 1 s, as indicated by the disappearance of these signals (~28−32 ppm) in both samples. After 1 s, an all-trans peak at ~34.3 ppm becomes apparent, particularly in the drawn sample. VanderHart and Khoury[44] identified this resonance with the monoclinic crystalline packing.[45] However, all-trans intensities between the orthorhombic and monoclinic shifts are also detectable in both samples after 1 s, and are quite significant in the drawn sample. Signals between the orthorhombic and monoclinic crystalline shifts have been attributed to intermediate components in UHMW−PE fibers by Kaji et al.[27] and in irradiated cross-linked polyolefin cable insulation by Harris and Alam.[33] These bands indicate disordered packing of the planes of all-trans chains. In the undrawn sample, the magnetization of these disordered all-trans signals is well relaxed by 10 s, and only a purely crystalline line shape is produced. However, in the drawn sample, the resonances are still visible after 10 s. By 60 s, the disordered all-trans magnetization is sufficiently relaxed, leaving only the sharp peaks of the orthorhombic and monoclinic crystals. Below, these data will be deconvoluted to produce "Torchia $T_{1,C}$ relaxation curves" of the morphological components.

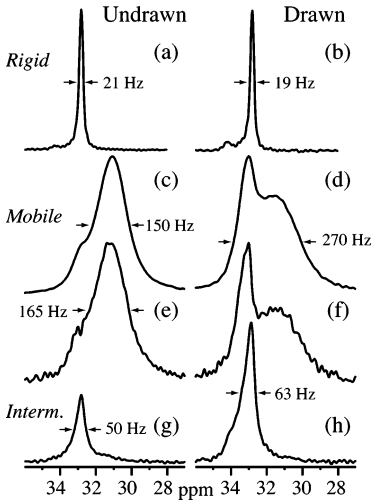

Figure 4. Comparison of selective spectra (based on the ^{13}C T_1) of the undrawn and drawn samples (left and right columns, respectively): (a, b) ^{13}C CP/MAS 60-s $T_{1,C}$ filtered spectra (rigid components); (c, d) ^{13}C DP/MAS with 0.7-s recycle delay (very mobile components); (e, f) ^{13}C CP/MAS 0.7-s inverse $T_{1,C}$ filtered spectra taken with the same experiment time as parts c and d (very mobile components); (g, h) difference spectra between ^{13}C CP/MAS 1- and 10-s $T_{1,C}$ filtered spectra (intermediate components).

On the basis of these Torchia experiments, selective ^{13}C spectra of the microstructural components were obtained. A $T_{1,C}$ filter time of $t_z = 60$ s was applied in the selection of long-$T_{1,C}$ components having very limited 75-MHz segmental motion (Figure 4, a and b). The 32.8-ppm peak of the orthorhombic signals, with a ~20-Hz full width at half-height, dominates the spectra; the monoclinic crystalline resonance at ~34.3 ppm is also seen clearly, particularly in the drawn sample. The formation of the metastable monoclinic crystalline form has been observed in the plastic deformation of polyethylenes and is described as a stress-induced "martensitic" transformation.[11,13,45] The resonances of disordered all-trans packing between the orthorhombic and monoclinic shifts have disappeared in the undrawn sample after $t_z = 60$ s (Figure 4a), but are still present in the drawn sample (Figure 4b). This indicates that less mobile (longer $T_{1,C}$) all-trans segments of disordered packing are present in the sample after cold drawing.

Inverse $T_{1,C}$-Filtered ^{13}C Spectra: Mobile Segments. Selection of the most mobile (short $T_{1,C}$) components is achieved by both simple ^{13}C direct-polarization (DP) MAS with a 0.7-s recycle delay (Figure 4, parts c and d) and ^{13}C CP/MAS with a 0.7-s inverse $T_{1,C}$ filter applied (Figure 4, parts e and f). The inverse $T_{1,C}$ filtered spectra were obtained as unscaled difference spectra, using a reference spectrum with $t_z = 1$ ms. The four spectra were all acquired in the same experiment time. Note that the inverse $T_{1,C}$ filtered spectrum in Figure 4e reproduces the line shape of the corresponding DP spectrum in Figure 4c. The line shape agreement between spectra in Figure 4, parts d and f, is not as good due to the enhanced CP efficiency and larger intensity of the intermediate-component signal, as observed in the increased intensity of the partly mobile all-trans peak (~33 ppm) in the drawn sample (Figure 4f).

As with the rigid components, cold drawing induces major changes in the fast-moving portions of the HDPE microstructure. The band of the amorphous components (about 28−32 ppm) seems to broaden, from ~150 to ~250 Hz, and shift slightly downfield, which was also seen in the CP/MAS spectra (Figure 2, parts c and d). A significant peak near 33 ppm (Figure 4, parts d and f) characteristic of the all-trans conformation appears in the drawn-sample spectra, with a chemical shift slightly

downfield of the orthorhombic crystal resonance. In contrast, in the undrawn sample only a small shoulder is observed in this spectral region (Figure 4, parts c and e). The line width of this mobile all-trans signal, ~90 Hz in Figure 4f, is much larger than that of the orthorhombic crystal resonance observed in Figure 4a. This indicates local disorder in conformation, or more likely, in chain packing. Various researchers have detected qualitatively similar mobile, all-trans resonances in high-strength PE fibers[27,46] and in irradiated cross-linked polyolefin cable insulation.[33] They have suggested such resonances to be due to an "interphase" [46] or "intermediate" component.[27,33] The mobile all-trans signal encompasses frequencies downfield from the orthorhombic peak position up to the monoclinic resonance, as noticed in the 60-s $T_{1,C}$ filtered spectrum of the drawn sample (Figure 4b).

We can isolate signals from chain segments in which the magnetization has relaxed after 1 s but long before the rigid crystalline core relaxes significantly, by using the generalized inverse $T_{1,C}$ filter described at the end of section 2.4, with $t_{za} = 1$ s and $t_{zb} = 10$ s. The resulting spectra originate from segments with ^{13}C T_1 times intermediate to the mobile amorphous and rigid crystalline domains. Spectra obtained as the difference between $t_{za} = 1$ s and $t_{zb} = 10$ s $T_{1,C}$ filtered signals are presented for both samples in Figure 4, parts g and h. These spectra, with peak widths of 50 and 63 Hz, respectively, retain only small intensity contributions from the well-ordered crystalline and gauche-containing amorphous phases. Figure 4 shows clearly that the intermediate component is intermediate not only in terms of $T_{1,C}$ but also in the line width: in the drawn sample, its signal is 3.3 times wider than the crystalline resonance, and 4 times narrower than the amorphous band. The chemical shift range (~32−34.4 ppm, Figure 4, parts g and h) shows that these chain segments have primarily all-trans conformations, while their relatively large line widths indicate significant disorder.

In terms of their intermediate $T_{1,C}$ relaxation times and distinctive MAS line shape, the all-trans chains with disordered packing represent a distinct fraction of chain segments having molecular conformation, packing, and mobility different from the crystalline and amorphous microstructures. In the case of the undrawn material, the presence of a minor third "intermediate" component with all-trans chains of disordered packing and significant mobility agrees with the observations of Strobl and Hagedorn[20] and numerous others.[26,30,47−50] The intermediate component in undeformed, melt-crystallized polyethylenes has been generally attributed to interfacial regions between the crystalline and amorphous domains. Whether the much larger intermediate component in the drawn sample is partly or exclusively interfacial has yet to be determined.

3.2. Characterization of the Intermediate Component(s) in the Drawn HDPE. To prove that the partially mobile and disordered all-trans segments are indeed distinct from crystalline and amorphous material, it must be further demonstrated that their properties are clearly different. Therefore, the amplitude of its segmental mobility and the degree of chain orientation have been characterized using 2D WISE and ^{13}C static experiments.

3.2.1. Mobility Characterization by 2D WISE. The motional amplitude of CH_2 groups can be estimated from their ^1H line width. Using 2D wide-line-separation (WISE) spectroscopy[23] in combination with the $T_{1,C}$ filtering methods discussed above, ^1H spectra of the various morphological components in the cold-drawn HDPE microstructure can be obtained. To eliminate effects of orientation in the necked material, the drawn sample was artificially made isotropic by carefully being cut into pieces about 2.5 mm in length along the draw direction. This size was small enough for the sample pieces to be randomly packed in the 4 mm diameter rotor, but large enough that the concentration of stress-induced microstructures like monoclinic crystals were not significantly enhanced due to cutting.

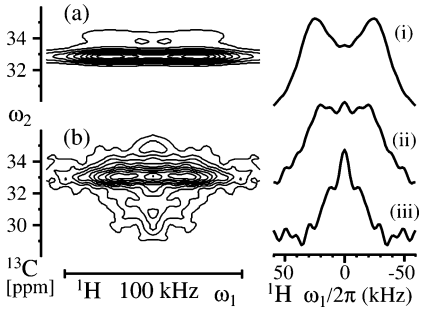

Figure 5. Two-dimensional $^1H-^{13}C$ WISE spectra of the cold-drawn HDPE sample made macroscopically isotropic in the rotor (a) with 10-s $T_{1,C}$ filter (crystalline) and (b) with 10-s inverse $T_{1,C}$ filter (amorphous and intermediate). Lee−Goldburg CP of 0.2 ms duration was employed in order to suppress ^1H spin diffusion. Contour lines are spaced at equal intervals, the interval being 10% of the maximum spectral intensity. ^1H wide line spectra obtained as cross sections at the orthorhombic crystalline (i), intermediate (ii), and amorphous (iii) ^{13}C signal maxima are displayed on the right.

In Figure 5, two-dimensional WISE spectra of the crystalline and mobile components selected by $T_{1,C}$ filtering are shown together with ^1H wide-line slices taken at the ^{13}C signal maxima. The ^1H wide-line spectrum of the orthorhombic crystallites (Figure 5i) at 32.8 ppm of ^{13}C is very wide, about 88 kHz full width at half-maximum, due to the strong $^1H-^1H$ dipolar couplings and only very limited fast motions. Also, the crystalline spectrum reveals two maxima reminiscent of a Pake pattern, which can be attributed to the geminal $^1H-^1H$ dipolar coupling.

Significant motional line narrowing is seen in the 10-s inverse $T_{1,C}$ filtered WISE spectrum (Figure 5b). The ^1H wide-line pattern of the amorphous-component cross section (Figure 5, part iii) at 30.6 ppm has a significantly reduced half-width of ~ 30 kHz as a result of high segmental mobility. The ^1H slice of the intermediate component(s) (Figure 5, part ii) at 33 ppm shows a full width of half-maximum of about 70 kHz, indicative of intermediate-amplitude fast motions ($>10^5$/s) of the segments. The motional narrowing by 70/88 = 0.8 corresponds to a motional amplitude of 20−40°.[51]

3.2.2. Mobility Characterization by ^{13}C Chemical Shift Anisotropy. A quantitative determination of the motional amplitude from WISE line shapes is challenging, due to the multispin character of the $^1H-^1H$ dipolar interactions. The effects of fast motions on the chemical shift anisotropy of the $^{13}CH_2$ groups are more amenable to a quantitative estimate of the motional amplitude. The chemical shift anisotropy in PE can be analyzed most easily with experiments without sample rotation, i.e., static NMR. To eliminate effects of sample orientation on the spectral line shape, a macroscopically isotropic sample was prepared by carefully cutting necked specimens into small flakes of "soap powder" texture, much finer than the sample used in the WISE experiments, as the artificially increased presence of stress-induced microstructures would not interfere much with probing local segment dynamics. These flakes were loosely packed into a 4 mm glass tube.

^{13}C static spectra of the undrawn and drawn "isotropic" samples are shown in Figure 6. The spectrum of the undrawn HDPE shows an ideal powder pattern, in particular for the crystalline material (Figure 6c). Calibration of the chemical shifts

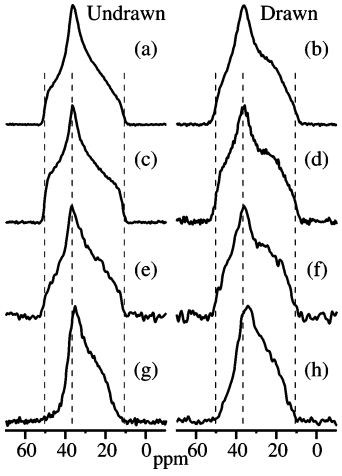

Figure 6. ^{13}C CP spectra (without sample rotation) of the undrawn and drawn samples unoriented with respect to the B_o field: (a, b) CP spectra; (c, d) 10-s $T_{1,C}$ filtered spectra (crystalline and long $T_{1,C}$ intermediate); (e, f) difference spectra between 1- and 10-s $T_{1,C}$ filtered spectra (intermediate); (g, h) 0.7-s inverse $T_{1,C}$ filtered spectra (amorphous and short $T_{1,C}$ intermediate).

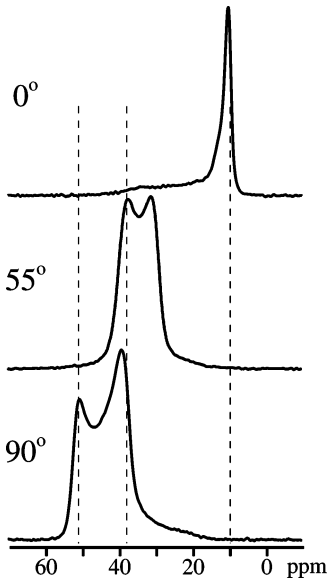

Figure 7. ^{13}C CP static spectra of the cold-drawn sample with draw axis oriented at various indicated angles with respect to the B_o field.

was verified by inspection of this spectrum (Figure 6c), in which the chemical shift principal values agreed with those determined by Schmidt-Rohr et al.[52] The crystalline spectrum of the artificially isotropic drawn sample (Figure 6d) exhibits some distortions from the ideal powder pattern, probably from residual macroscopic orientation. The distortion near 20 ppm cannot be explained by variations of the σ_{33} chemical shift principal value (near 10 ppm) with chain packing;[39] this is confirmed by the absence of a peak near 20 ppm in spectra of the drawn sample, Figure 7 (top trace).

The line shapes of the intermediate-component spectra for both the undrawn and drawn samples (Figure 6, parts e and f, respectively) exclude unhindered rotations around the chain axis (as would be found in a "rotator phase"), which would yield a powder pattern with a peak, not a shoulder, on the downfield (left-hand) side of the spectrum. In general, fast motions around the chain axis, i.e., around the σ_{33} direction, manifest themselves by a reduced difference between the two perpendicular principal values $\bar{\sigma}_{11}$ and $\bar{\sigma}_{22}$ of the motionally averaged chemical shift tensor. They are related to the rigid-limit values σ_{11}, σ_{22} and the rotation angle ϕ according to[53]

$$\bar{\sigma}_{11} = -(^1/_2)\{\delta - (\sigma_{11} - \sigma_{22})\langle\cos(2\phi)\rangle\} + \sigma_{iso} \quad (2a)$$

$$\bar{\sigma}_{22} = -(^1/_2)\{\delta + (\sigma_{11} - \sigma_{22})\langle\cos(2\phi)\rangle\} + \sigma_{iso} \quad (2b)$$

with

$$\delta = \sigma_{33} - \sigma_{iso} \quad (2c)$$

The pointed brackets indicate the averaging of the rotation angle around the chain axis. As a result

$$\langle\cos(2\phi)\rangle = (\bar{\sigma}_{11} - \bar{\sigma}_{22})/(\sigma_{11} - \sigma_{22}) \quad (3)$$

For small rotation angles, the left-hand-side of eq 3 can be expanded to yield the root-mean-square (rms) rotation angle $\langle\phi^2\rangle^{1/2}$ (in degrees):

$$\langle\phi^2\rangle^{1/2} = \sqrt{2\{1 - (\bar{\sigma}_{11} - \bar{\sigma}_{22})/(\sigma_{11} - \sigma_{22})\}} \times 180°/\pi \quad (4)$$

While the modified ^{1}H line shape in WISE NMR and the shortened $T_{1,C}$ indicate molecular mobility of the intermediate component(s) in the drawn sample, the spectrum of Figure 6f shows only limited motional line narrowing. Nevertheless, the powder spectrum is consistent with a reduction in $(\bar{\sigma}_{11} - \bar{\sigma}_{22})/(\sigma_{11} - \sigma_{22})$ by 5% (0.7 ppm), which would correspond to $\langle\phi^2\rangle^{1/2} = 18°$ according to eq 4. This should be compared with the 6° amplitude rotational motion occurring even in the cores of PE crystallites at ambient temperature.[54] Note that fast chain flips by 180° would leave the chemical shift tensor invariant, but would reduce the long-range ^{1}H−^{1}H dipolar couplings.[55] However, sharpening of the Pake horns in the WISE spectrum (Figure 5, part ii) would be expected to result from the weakening of the long-range dipolar couplings, but it is not observed.

3.2.3. Degree of Orientation. ^{13}C static NMR experiments were also used to characterize the degree of chain orientation in the major components of the cold-drawn sample. The draw axes of pieces of the necked specimens were aligned at 0°, 55°, and 90° to the external magnetic field B_o (for details see the Experimental Section) in order to analyze the molecular orientation distribution. VanderHart and Khoury[44] performed similar experiments on drawn PE, but without selection and detailed analysis of the intermediate component(s).

Simple CP spectra acquired at the various angles of sample alignment are presented in Figure 7. Selective spectra based on $T_{1,C}$ filtering schemes are displayed in Figure 8. The spectra for the 0° orientation are easiest to interpret. A sharp peak at the $\sigma_{33} = 10$ ppm edge of the chemical-shift anisotropy was observed for the long- and intermediate-$T_{1,C}$ components. This peak indicates good alignment of the local chain axes, which coincide with the σ_{33} principal axis of the chemical shift tensor, with the B_0 field, and thus with the draw direction. In contrast, the amorphous spectra show poor chain orientation with the draw axis, except for a relatively small contribution near 13 ppm that probably arises from the intermediate component with the shortest $T_{1,C}$.

A spreading of the σ_{33} peak intensity indicates a distribution of chain orientations relative to the B_0 field and draw direction. At the same time, some broadening can also arise from variations in the σ_{33} principal value of the chemical shift tensor with chain packing.[39] Therefore, simulations of spectra at all three sample orientations were performed for the crystalline and intermediate components and are shown in Figure 8. For the

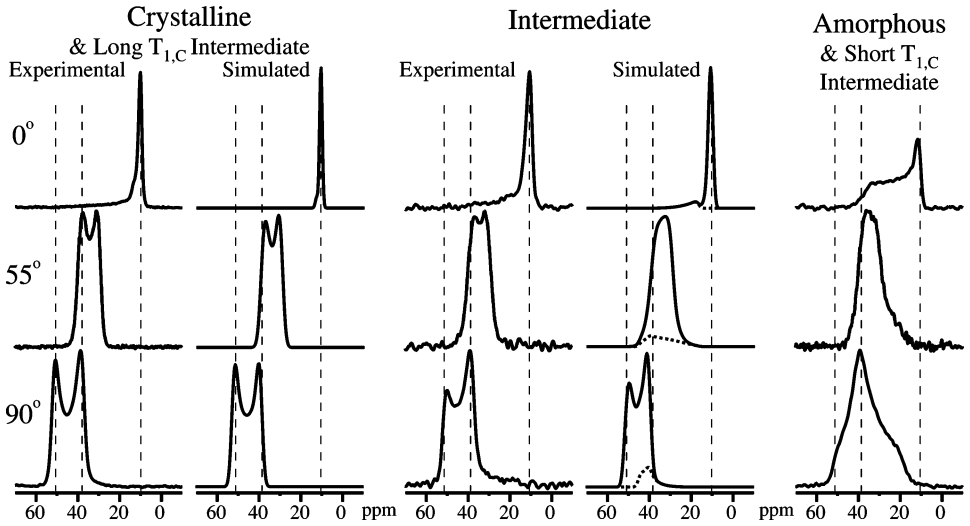

Figure 8. Selective ^{13}C CP static spectra of the drawn sample with draw axis oriented at various indicated angles with respect to the B_o field. Both experimental and simulated spectra are shown for the rigid and intermediate components. Details of the simulation parameters are described in the text. Experimental spectra: crystalline and long $T_{1,C}$ intermediate components (10-s $T_{1,C}$ filtered spectra); intermediate component (difference between 1- and 10-s $T_{1,C}$ filtered spectra); amorphous and short $T_{1,C}$ intermediate components (0.7-s inverse $T_{1,C}$ filtered spectra). In the simulated spectra of the intermediate component, the dashed spectra represent the less oriented and more mobile portion (ca. 10%), as mentioned in the text.

orthorhombic crystal, principal values of 51, 38, and 10 ppm were used, giving an isotropic chemical shift of 33 ppm. The root-mean-square (rms) width of the Gaussian distribution of the crystalline component was $\sigma = 1 \pm 1°$. In the 0°-orientation simulation for the crystalline component, a contribution of 7% from the monoclinic crystalline material (using $\sigma_{33} = 12$ ppm) was included.

The intermediate-component spectra roughly resemble those of the crystallites; in particular, this confirms the all-trans conformation of the intermediate component(s). The orientation distribution used to simulate the intermediate-component spectra in Figure 8 consisted of Gaussians with $\sigma = 1°$ to 8°, with equal weights. With increasing σ, the difference between σ_{11} and σ_{22} was gradually reduced in the simulation, modeling more motional freedom around the chain axis. In addition, a 10% contribution of a more mobile intermediate component with $\sigma = 20°$ and principal values of 44, 39, and 16 ppm (reduced spread due to rotations around the chain axis and some chain-axis motions) had to be included to produce an acceptable simultaneous simulation of the spectra at all three orientations. It is indicated by dashed lines in the simulated spectra of Figure 8. The rms angle of the overall distribution of chain axes in the intermediate components is $8 \pm 3°$.

3.3. Morphological Component Quantification by NMR.

3.3.1. Torchia Curves and Deconvolution. To quantify different components in direct-polarization ^{13}C NMR, appropriate values for the recycle delay must be established. These are best determined by observing the ^{13}C T_1 relaxation of the various morphological components in the HDPE material, using the Torchia ^{13}C T_1 relaxation experiment[34] described in the context of Figure 3. Plotting the spectral areas as a function of the $T_{1,C}$ filter time yields "Torchia $T_{1,C}$ relaxation curves".[26−28,40,43] Torchia $T_{1,C}$ relaxation curves distinct to the crystalline, intermediate, and amorphous phases can be obtained through spectral deconvolution. The noncrystalline ^{13}C signals that have not relaxed within a certain time t_z can be estimated using an extension of the inverse $T_{1,C}$ filter: A pair of CP/MAS $T_{1,C}$ filtered spectra are acquired with the same number of scans, one with a filter delay t_z, the other with a longer filter time that leaves only crystalline signals (10 s for the undrawn, melt-crystallized HDPE, Figure 3). The crystalline spectrum is then manually scaled to leave a smooth difference between the two spectra, i.e., such that the sharp orthorhombic crystal peak at 32.8 ppm is minimized in the residual.

The difference spectrum thus obtained approximates the noncrystalline ^{13}C signals that survive a specific $T_{1,C}$ filter time t_z, since all the crystalline components have been subtracted out. If the amorphous portion of the difference spectrum is taken at chemical shifts < 32 ppm (the gauche-containing region[38]), the remainder of the spectral area is a good estimate of the all-trans intermediate-component signals. The validity of this deconvolution is confirmed by the linear (i.e., exponential) initial time dependence of the intermediate-component $T_{1,C}$ relaxation data obtained in this way, see Figure 9d, which continues without a break at times greater than 1 s where the signals of the gauche-containing fraction have disappeared. The integrated intensity of crystalline signals is also obtained in this deconvolution procedure.

The resulting Torchia $T_{1,C}$ relaxation curves for the morphological components in both the undrawn and cold-drawn HDPE samples are displayed in Figure 9. It is clear that the crystalline signals in the drawn sample relax much faster than in the undrawn precursor. This faster $T_{1,C}$ relaxation indicates crystallites of smaller thickness in the cold-drawn, necked material.[40] In contrast, intermediate-component ^{13}C magnetization in the cold-drawn material relaxes considerably slower, and from a relatively higher initial value, than in the undeformed material. This behavior is consistent with observations made in Figure 3, where the all-trans resonances intermediate to the orthorhombic and monoclinic shifts were extinct in the undrawn sample by 10 s, but still present in the drawn sample until 60 s.

Our analysis is based on the intermediate component having shorter $T_{1,C}$ values than the crystal, but it does not assume that any component has a single $T_{1,C}$. Chain (and spin) diffusion from the amorphous to the crystalline domains dominates the $T_{1,C}$ relaxation in the crystallites,[42] due to the very long intrinsic $T_{1,C}$ of crystalline PE. The closer a certain region in the crystal is to the amorphous regions, the faster the diffusion-mediated $T_{1,C}$ relaxation of segments observed while residing in this region (note that the observation time is much shorter than the shortest $T_{1,C}$). Therefore, the shortest-$T_{1,C}$ signals of the crystal, which

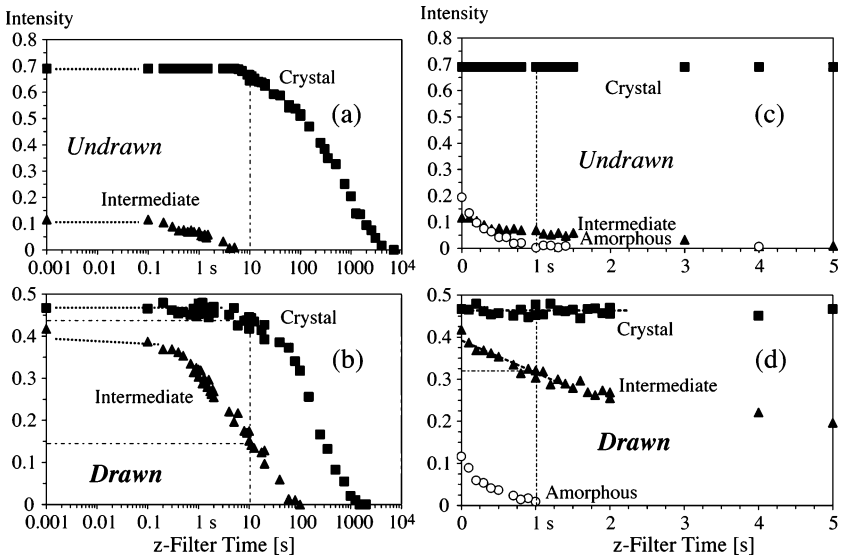

Figure 9. Torchia ^{13}C T_1 relaxation curves of the major morphological components in the undrawn (a, c) and cold-drawn (b, d) HDPE samples; crystalline (filled squares); intermediate (filled triangles); amorphous (open circles). Intensities are spectral areas relative to the original 1 ms CP/$T_{1,C}$ filtered spectrum of all components. The amorphous fraction is underrepresented here relative to its true amount due to differences in CP efficiencies. It is fully quantified from DP data, with some corrections as described in the text.

will be included in the intermediate components, are from chain segments observed near the crystalline−amorphous interface, which has indeed been shown to have an intermediate degree of order.

3.3.2. Component Quantification for the Undrawn HDPE. Direct-polarization (DP) ^{13}C NMR can be used to quantify the mass fractions of mobile and rigid components in polyethylenes if full $T_{1,C}$ relaxation of the components during the recycle delay is achieved.[46] The crystalline phase in polyethylene can have extremely long $T_{1,C}$ times, on the order of 10^2-10^3 s.[26,40,41] Since the noncrystalline component produces only a low and broad signal, acquiring a fully relaxed spectrum of the HDPE sample with good noncrystalline signal would require unreasonably long experiment times. In addition, the resonances of the crystalline and noncrystalline phases overlap in an unfiltered spectrum.

These problems are overcome by combining ^{13}C DP/MAS spectra with different recycle delays and numbers of scans as outlined by Hu and Schmidt-Rohr[46] in their study of UHMW−PE fibers. A short recycle delay (~1 s) yields signals primarily from the very mobile regions. Longer delays give spectra that are a superposition of the components whose ^{13}C magnetization has sufficiently relaxed during the delay time. Spectra with short recycle delays are acquired with a large number of scans to measure the mobile signals (i.e., amorphous, short $T_{1,C}$ intermediate) with good sensitivity. Spectra with very long delays are obtained with few scans, keeping the experiment time within acceptable limits.

The Torchia $T_{1,C}$ relaxation curves of the undrawn HDPE material in Figure 9, parts a and c show that the amorphous and intermediate components have essentially relaxed away in 1 and 5 s, respectively. Only about 2% of the crystalline signals remain unrelaxed after 4000 s. Hence, values of 1, 10, and 4000 s were selected for the DP recycle delays. The NMR component composition results obtained with these recycle delays are given in Table 1, along with corresponding data measured with Raman scattering and DSC. The method of Strobl and Hagedorn[20] to quantify the intermediate component in PE was applied in the analysis of the Raman scattering measurements. Good agreement between the three techniques is found. The mass fraction of the intermediate component derived from the NMR and Raman scattering measurements is comparable to other studies[20,47] of slow-cooled, melt-crystallized linear polyethylene, and falls in line with the value predicted by Mandelkern and Peacock[56] based on the molecular weight of the HDPE analyzed. Residual stresses induced by the compression-molding process may be present in the undrawn HDPE sample. These can promote formation of metastable phases such as the monoclinic crystalline form observed at ~34.3 ppm in the CP/MAS $T_{1,C}$ filtered spectrum (Figure 4a).

Table 1. Comparison of Morphological Component Quantities (mass %) in the Undrawn, Melt-Crystallized HDPE Material Obtained with Various Analytical Techniques[a]

analytical technique	crystalline	intermediate	amorphous
solid-state NMR	62 ± 2	10 ± 2	28 ± 2
Raman scattering	62 ± 2	8 ± 3	30 ± 3
DSC	64 ± 2		

[a] The experimental methods used with each technique are described in the text.

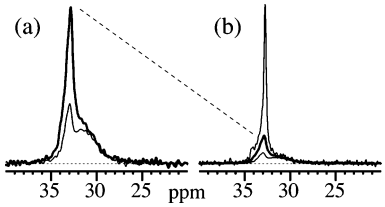

Figure 10. Demonstration of the quantitative ^{13}C DP/MAS procedure introduced by Hu and Schmidt-Rohr[46] to measure component composition in polyethylene. Spectra are of the cold-drawn HDPE sample. Three DP spectra acquired with different recycle delays and numbers of scans are shown in two sets: (a) 1 s (1024 scans) and 10 s (512 scans); (b) 2000 s (32 scans) and the two spectra of part a. For direct comparison, spectra are scaled to compensate for the different number of scans. The 10-s spectrum is indicated by a thick line in both sets. The transient heteronuclear NOE was suppressed in all DP experiments used in the quantitative procedure.

3.3.3. Quantitative ^{13}C NMR for Drawn HDPE. Application of the NMR quantification method in ref 46 to the cold-drawn HDPE is presented in Figure 10. Three spectra with different recycle delays are shown, scaled to account for the number of scans. Thirty-two scans of the fully relaxed signal with a recycle delay of 2000 s were recorded (Figure 10b, top thin line). While the all-trans peak near 32.8 ppm and a small downfield peak from the monoclinic crystal modification are

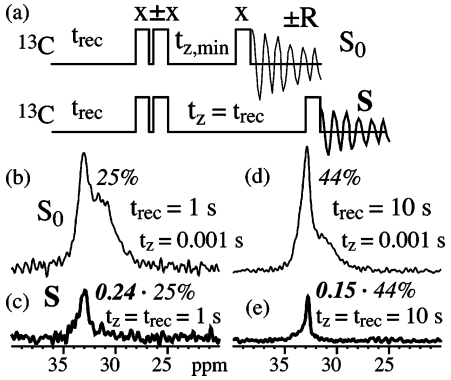

Figure 11. (a) Pulse sequence for ^{13}C direct polarization (DP) NMR followed by a $T_{1,C}$ filter, used to correct for "contamination" of the ^{13}C signals in DP experiments by longer-T_1 components, as described in the text. The full reference spectrum is obtained with the minimal $T_{1,C}$ filter time t_z (top), the spectrum of the slowly relaxing components with a longer filter time of $t_z = t_{rec}$ (bottom). Recycle delays employed for the spectral pairs shown were (b, c) 1 and (d, e) 10 s. The spectrum with the largest intensity in each pair was obtained with a very short $T_{1,C}$ filter time (1 ms), while the spectrum of smaller area was acquired with a $T_{1,C}$ filter equal to the recycle delay t_{rec}.

clearly seen, the low amorphous signals are not well-defined due to noise and peak overlap. Together with the mobile all-trans signals of the intermediate component, the amorphous phase magnetization is observed fully relaxed with a shorter recycle delay of 10 s and many more scans (thick lines in Figure 10, parts a and b). A 1-s DP spectrum with suppression of the transient heteronuclear Overhauser effect (NOE)[46] (thin line in Figure 10a) also gives the fully relaxed amorphous magnetization, along with a short-$T_{1,C}$ intermediate component resonance near 33 ppm. The scan-normalized area of the 1-s spectrum, relative to the total area after 2000 s, is 25%. This value is a first approximation to the amorphous mass fraction. The area fraction of the 10-s spectrum, 44%, is a first estimate of the sum of amorphous and intermediate components.

3.3.4. Component Quantification for the Drawn HDPE. To separate the major components in the cold-drawn HDPE more reliably, the Torchia $T_{1,C}$ relaxation data of Figure 9, parts b and d, were taken into account in the spectral deconvolution. The intermediate component can be quantified most reliably from the intermediate-to-crystalline ratio, $(40 \pm 3)/(47 \pm 2)$, as determined from the extrapolated initial values (at $t_z = 0$) of the Torchia curves in Figure 9b. This quantification assumes equal cross-polarization efficiencies of the intermediate and crystalline components, which is justified given the similar dipolar coupling strengths observed in the WISE spectra (Figure 5). If this assumption were wrong, the intermediate fraction would be underrepresented and therefore even slightly larger.

The intermediate-to-crystalline ratio is useful, but for a full analysis the amorphous component needs to be quantified as well. In the curves of Figure 9, parts c and d, the amorphous signals in the undrawn and drawn samples show similar behavior and are sufficiently relaxed by 1 s. However, Figure 9d also shows that within $t_z = 1$ s, the intermediate component relaxes significantly as well and therefore "contaminates" the 33-ppm band in the 1-s spectrum of Figure 10. How large this contribution is can be estimated using the scheme shown in Figure 11a, where the DP/MAS experiment has been extended by a $T_{1,C}$ filter which selectively retains magnetization with long $T_{1,C}$. Indeed, for a recycle delay of 1 s, comparison of the spectra in Figure 11, parts b and c, which were obtained with $T_{1,C}$ filter times of 0.001 and 1 s, respectively, reveals an intermediate component that contributes to the $t_{rec} = 1$-s spectrum. It accounts for 0.24 of the peak area and needs to be subtracted from the amorphous fraction. The true intermediate-component contribution is even larger, given that the $T_{1,C}$ curve in Figure 9d shows that the intermediate component has relaxed by 0.32/0.42 = 0.76 (see the dash−dotted line). In other words, the intermediate-component contribution to the 1-s DP spectrum in Figure 10a or 11b is 0.24/0.76 = 0.32, or about one-third. As a result, the amorphous mass fraction is not the full 25% estimated above from Figure 10, but only $(1 - 0.32) \times 25\% = 17\%$. Combined with the intermediate-to-crystalline ratio, $(40 \pm 3)/(47 \pm 2)$, determined above, this gives an intermediate fraction of $38 \pm 3\%$.

Table 2. Comparison of Morphological Component Quantities (mass %) Obtained by NMR in the Undrawn and Cold-Drawn HDPE Samples[a]

HDPE sample	orthorhombic crystalline	monoclinic crystalline	intermediate	amorphous
undrawn	59 ± 2	3 ± 1	10 ± 2	28 ± 2
cold-drawn	41 ± 4	4 ± 2	38 ± 6	17 ± 4

[a] The error margins take into account uncertainties in the exact boundaries between the different fractions.

Alternatively, we can estimate the intermediate-component mass fraction from the ^{13}C DP/MAS spectrum with 10-s recycle delay (Figure 10, 44% area fraction), correcting for the total amorphous component (−17%), the crystalline fraction that has already relaxed within this time (4% according to Figure 9b), and the intermediate fraction that has not yet fully relaxed within 10 s (correct by multiplying with 40%/(40% − 15%) = 1.6, according to Figure 9b). The resulting percentage of the intermediate fraction, $(44\% - 17\% - 4\%) \times 1.6 = 37 \pm 4\%$, agrees well with the value of $38 \pm 3\%$ determined above.

3.3.5. Synopsis of Component Quantification. The mass-percentages of the various morphological components in the undrawn and cold-drawn HDPE samples from our analysis are summarized in Table 2. The error margins for the drawn sample include uncertainties in the exact delineation between components. The monoclinic fraction was derived from the monoclinic-to-orthorhombic peak-area ratio in a 10-s $T_{1,C}$ filtered CP/MAS spectrum for the undrawn sample and a 60-s $T_{1,C}$ filtered CP/MAS spectrum for the drawn sample; see Figure 3.

Table 2 highlights the significant differences observed between the undrawn and cold-drawn material. Overall crystallinity is clearly smaller in the cold-drawn and necked HDPE ($45 \pm 4\%$ compared to $62 \pm 2\%$ in the undeformed precursor). At the same time, the amorphous content has been diminished, consistent with the reduction in the amorphous signal intensities in the ^{1}H and ^{13}C CP/MAS spectra of Figure 2. Most important, however, is the dramatically larger fraction ($38 \pm 6\%$) of the intermediate component(s) in the cold-drawn HDPE. This quantity is greater than the contributions from the amorphous domains and the monoclinic crystalline material. Hence, the partially mobile and oriented all-trans chains of the intermediate component(s) comprise a noteworthy part of the cold-drawn microstructure that should not be ignored in component modeling. As indicated throughout the text, they possibly contain contributions from several distinct morphological components, such as interfacial segments, isolated tie molecules, tie−molecule bundles, and/or small disordered crystallites.

Like almost any quantification of the morphological composition of melt-crystallized semicrystalline polymers, our analysis does not imply sharp boundaries between the various components. In other words, it is in keeping with the component analysis in standard undrawn polyethylene. There, the accepted model is one of continuous disorder, from the ordered crystal

through the partially ordered interfacial segments to the noncrystalline regions. Nevertheless, for decades it has been the accepted and fruitful procedure to use a two- or three-component analysis, with component fractions (in particular crystallinities) considered accurate within a few %. Indeed, the results from different methods usually agree quite well, compare, for instance, Raman and NMR component fractions in Table 1.

4. Summary and Outlook

Through several one- and two-dimensional solid-state NMR experiments, a major fraction of chain segments that are distinct from the crystalline and amorphous material has been identified in cold-drawn high-density polyethylene. CP/MAS experiments utilizing an inverse $T_{1,C}$ filter show signals with chemical shifts characteristic of all-trans chain conformations and intermediate ^{13}C T_1 values. The lines of the intermediate components in the drawn and undrawn samples are much broader than those of the crystalline peaks, indicating disorder in chain packing. Studies of the segmental motions and orientational order further corroborated the distinction between the crystalline and intermediate components in the cold-drawn material. The intermediate-component chain segments undergo intermediate-amplitude ($\sim$20°) motions around the chain axis, according to the wide-line narrowing detected in the inverse $T_{1,C}$ filtered WISE spectrum and ^{13}C NMR experiments without sample spinning. Chains in the intermediate component(s) are generally aligned with the draw direction, but with a wider orientation distribution of $\sigma = 8°$ relative to the crystalline chains with $\sigma = 1°$. The component morphology has been quantified by ^{13}C NMR and detailed relaxation-time analysis, and the intermediate components have been found to comprise 38 $\pm$ 6% of all chain segments in the bulk.

The findings reported here open a new perspective on the component structure of cold-drawn high-density polyethylene. With the mobile all-trans segments identified as distinct from the crystalline and amorphous phases and making up almost 40% of the sample, many questions can be asked. What is the location of the intermediate components in the microstructure, and what are their dimensions? How are they related to tie molecules? What role do they play in the drawing process? What is the effect of drawing temperature and strain rate on the development of the intermediate component? Some of these questions will be addressed in forthcoming studies.

Acknowledgment. The authors wish to thank the Alfred P. Sloan Foundation and NSF/MRSEC for support of this work. D.M.M. thanks S. L. Hsu and A. Heintz for access to and assistance with the Raman scattering equipment. Also thanks are due to A. Heintz for assistance with the Raman spectroscopic method to determine phase composition.

References and Notes

(1) Takayanagi, M.; Imada, K.; Kajiyama, T. *J. Polym. Sci.: Part C* **1966**, *15*, 263.
(2) Ward, I. M., Ed. *Developments in oriented polymers*—1; Applied Science Publishers Ltd.: Barking, Essex, England, 1982.
(3) Peterlin, A. *Colloid Polym. Sci.* **1987**, *265*, 357.
(4) Ward, I. M., Ed. *Developments in oriented polymers*—2; Elsevier Applied Science Publishers Ltd.: Barking, Essex, England, 1987.
(5) Ward, I. M.; Hadley, D. W. *An Introduction to the Mechanical Properties of Solid Polymers*; John Wiley & Sons: New York, 1993.
(6) O'Connell, P. A.; Bonner, M. J.; Duckett, R. A.; Ward, I. M. *Polymer* **1995**, *36*, 2355.
(7) Lagarón, J. M.; Dixon, N. M.; Gerrard, D. L.; Reed, W.; Kip, B. J. *Macromolecules* **1998**, *31*, 5845.
(8) Lagaron, J. M.; Dixon, N. M.; Reed, W.; Pastor, J. M.; Kip, B. J. *Polymer* **1999**, *40*, 2569.
(9) Cawood, M. J.; Channell, A. D.; Capaccio, G. *Polymer* **1993**, *34*, 423.
(10) Peterlin, A. *J. Mater. Sci.* **1971**, *6*, 490.
(11) Bowden, P. B.; Young, R. J. *J. Mater. Sci.* **1974**, *9*, 2034.
(12) Peterlin, A. *Colloid Polym. Sci.* **1975**, *253*, 809.
(13) Lin, L.; Argon, A. S. *J. Mater. Sci.* **1994**, *29*, 294.
(14) Hiss, R.; Hobeika, S.; Lynn, C.; Strobl, G. *Macromolecules* **1999**, *32*, 4390.
(15) Gibson, A. G.; Davies, G. R.; Ward, I. M. *Polymer* **1978**, *19*, 683.
(16) Rodríguez-Cabello, J. C.; Martín-Monge, J.; Lagarón, J. M.; Pastor, J. M. *Macromol. Chem. Phys.* **1998**, *199*, 2767.
(17) Lagarón, J. M.; López-Quintana, S.; Rodriguez-Cabello, J. C.; Merino, J. C.; Pastor, J. M. *Polymer* **2000**, *41*, 2999.
(18) Popli, R.; Mandelkern, L. *J. Polym. Sci.: Part B: Polym. Phys.* **1987**, *25*, 441.
(19) Wunderlich, B. *Macromolecular Physics*; Academic Press: New York, 1973; Vol. 1.
(20) Strobl, G. R.; Hagedorn, W. *J. Polym. Sci.: Polym. Phys. Ed.* **1978**, *16*, 1181.
(21) Rull, F.; Prieto, A. C.; Casado, J. M.; Sobron, F.; Edwards, H. G. M. *J. Raman Spectrosc.* **1993**, *24*, 545.
(22) Bennett, A. E.; Rienstra, C. M.; Auger, M.; Lakshmi, K. V.; Griffin, R. G. *J. Chem. Phys.* **1995**, *103*, 6951.
(23) Schmidt-Rohr, K.; Clauss, J.; Spiess, H. W. *Macromolecules* **1992**, *25*, 3273.
(24) Lee, M.; Goldburg, W. I. *Phys. Rev.* **1965**, *140*, A1261.
(25) van Rossum, B.-J.; de Groot, C. P.; Ladizhansky, V.; Vega, S.; de Groot, H. J. M. *J. Am. Chem. Soc.* **2000**, *122*, 3465.
(26) Kitamaru, R.; Horii, F.; Murayama, K. *Macromolecules* **1986**, *19*, 636.
(27) Kaji, A.; Ohta, Y.; Yasuda, H.; Murano, M. *Polym. J.* **1990**, *22*, 455.
(28) Kaji, A.; Yamanaka, A.; Murano, M. *Polym. J.* **1990**, *22*, 893.
(29) Chen, W.; Fu, Y.; Wunderlich, B.; Cheng, J. *J. Polym. Sci.: Part B: Polym. Phys.* **1994**, *32*, 2661.
(30) Cheng, J.; Fone, M.; Reddy, V. N.; Schwartz, K. B.; Fisher, H. B.; Wunderlich, B. *J. Polym. Sci.: Part B: Polym. Phys.* **1994**, *32*, 2683.
(31) Fu, Y.; Chen, W.; Pyda, M.; Londono, D.; Annis, B.; Boller, A.; Habenschuss, A.; Cheng, J.; Wunderlich, B. *J. Macromol. Sci.—Phys.* **1996**, *B35*, 37.
(32) Cheng, J.; Fone, M.; Fu, Y.; Chen, W. *J. Therm. Anal.* **1996**, *47*, 673.
(33) Harris, D. J.; Alam, M. K. *Polymer* **2002**, *43*, 5147.
(34) Torchia, D. A. *J. Magn. Reson.* **1978**, *30*, 613.
(35) Wilson, C. W.; Pake, G. E. *J. Chem. Phys.* **1957**, *27*, 115.
(36) Smith, J. B.; Manuel, A. J.; Ward, I. M. *Polymer* **1975**, *16*, 57.
(37) Kitamaru, R.; Horii, F. *Adv. Polym. Sci.* **1978**, *26*, 138.
(38) Earl, W. L.; VanderHart, D. L. *Macromolecules* **1979**, *12*, 762.
(39) VanderHart, D. L. *J. Magn. Reson.* **1981**, *44*, 117.
(40) Axelson, D. E.; Mandelkern, L.; Popli, R.; Mathieu, P. *J. Polym. Sci.: Polym. Phys. Ed.* **1983**, *21*, 2319.
(41) Axelson, D. E. In *High-Resolution NMR Spectroscopy of Synthetic Polymers in Bulk*; Komoroski, R. A., Ed.; VCH Publishers: Deerfield Beach, FL, 1986; p 157.
(42) Schmidt-Rohr, K.; Spiess, H. W. *Macromolecules* **1991**, *24*, 5288.
(43) Kuwabara, K.; Kaji, H.; Horii, F.; Bassett, D. C.; Olley, R. H. *Macromolecules* **1997**, *30*, 7516.
(44) VanderHart, D. L.; Khoury, F. *Polymer* **1984**, *25*, 1589.
(45) Seto, T.; Hara, T.; Tanaka, K. *Jpn. J. Appl. Phys.* **1968**, *7*, 31.
(46) Hu, W.-G.; Schmidt-Rohr, K. *Polymer* **2000**, *41*, 2979.
(47) Glotin, M.; Mandelkern, L. *Colloid Polym. Sci.* **1982**, *260*, 182.
(48) Shen, C.; Peacock, A. J.; Alamo, R. G.; Vickers, T. J.; Mandelkern, L.; Mann, C. K. *Appl. Spectrosc.* **1992**, *46*, 1226.
(49) Mutter, R.; Stille, W.; Strobl, G. *J. Polym. Sci.: Part B: Polym. Phys.* **1993**, *31*, 99.
(50) Baker, A. M. E.; Windle, A. H. *Polymer* **2001**, *42*, 667.
(51) Hentschel, R.; Sillescu, H.; Spiess, H. W. *Polymer* **1981**, *22*, 1516.
(52) Schmidt-Rohr, K.; Wilhelm, M.; Johansson, A.; Spiess, H. W. *Magn. Reson. Chem.* **1993**, *31*, 352.
(53) Schmidt-Rohr, K.; Spiess, H. W. *Multidimensional Solid-State NMR and Polymers*; Academic Press: San Diego, CA, 1994.
(54) Hentschel, D.; Sillescu, H.; Spiess, H. W. *Makromol. Chem.* **1979**, *180*, 241.
(55) Hu, W.-G.; Boeffel, C.; Schmidt-Rohr, K. *Macromolecules* **1999**, *32*, 1611.
(56) Mandelkern, L.; Peacock, A. J. *Stud. Phys. Theor. Chem.* **1988**, *54*, 201.

MA0513517